Proceedings of the Combustion Institute, Volume 28, 2000/pp. 2063–2070

# CHARACTERIZATION OF A COFLOWING METHANE/AIR NON-PREMIXED FLAME WITH COMPUTER MODELING, RAYLEIGH-RAMAN IMAGING, AND ON-LINE MASS SPECTROMETRY

CHARLES S. MCENALLY,[1] LISA D. PFEFFERLE,[1] ANDREW M. SCHAFFER,[1] MARSHALL B. LONG,[1] RAHIMA K. MOHAMMED,[1] MITCHELL D. SMOOKE[1] AND MEREDITH B. COLKET[2]

[1]*Center for Combustion Studies*
*Yale University*
*New Haven CT 06520-8286, USA*
[2]*United Technologies Research Center*
*East Hartford CT 06108, USA*

A non-sooting lifted methane/air coflowing non-premixed flame has been studied experimentally and computationally. The flame structure was computed using a model that solves the fully elliptic governing equations, utilizes detailed transport coefficients and a chemical kinetic mechanism with $C_1$ to $C_6$ hydrocarbons, and includes an optically thin radiation submodel. Gas temperature, major species mole fractions, and non-fuel hydrocarbon concentrations were experimentally mapped in two dimensions with both probe techniques (thermocouples and on-line mass spectrometry) and optical diagnostics (Rayleigh and Raman scattering). A differential polarization strategy was used to remove $C_2$ and polycyclic hydrocarbon fluorescence interferences from the Raman scattering signals, which dramatically improved the quality of the laser diagnostic images over what had previously been possible. Good agreement was observed between the probe and laser images; this validates the Rayleigh-Raman data processing procedure, and it shows that the probes produce negligible perturbations to the flame structure. The spatial precision of the data and range of measured quantities provides a sensitive test of the computations. Nonetheless, the model reproduces most of the experimental observations, including the overall flame height and liftoff height, the peak concentrations and spatial distributions of major species, and the peak concentrations of oxygenated hydrocarbon intermediates such as ketene and soot precursors such as benzene and acetylene.

## Introduction

An important goal of combustion science is to develop computational models based on fundamental principles that are applicable to practical combustors and are capable of predicting chemically complex phenomena such as soot formation. Currently, flame models that incorporate detailed chemistry are well developed for one-dimensional configurations and are being extended toward multidimensional systems [1–6]. These models depend upon a large number of parameters that have non-zero uncertainties (transport coefficients, thermodynamic properties, rate constants), so detailed comparison of model results with experimental data is necessary to validate the models [7].

The objective of the current study was to apply state-of-the-art experimental and computational methods to a well-defined axisymmetric laminar coflowing methane/air non-premixed flame so that we could determine how sensitive of an experimental test of the model was possible, and whether the model could meet this test. To some degree this work is an extension of an earlier study where we compared model predictions with temperature and major species images obtained from Rayleigh-Raman scattering [1]. The detailed chemical kinetic mechanism in the model has been enlarged to include hydrocarbons as large as benzene ($C_6H_6$), and the Rayleigh-Raman procedure has been modified to use polarization information to subtract fluorescence interferences, which results in dramatically improved images. Also, additional thermocouple and mass spectrometric measurements of temperature, major species, and non-fuel hydrocarbons have been included to determine quantities not amenable to laser diagnostics and to allow us to compare *in situ* and probe measurements.

## Computational and Experimental Methods

### *Flame Configuration*

The fuel, which consisted of 65 mol % methane in nitrogen, flowed from a 0.4 cm inner diameter vertical tube, and the oxidizer, air, flowed from the annular region between this tube and a 5.0 cm inner diameter concentric tube. The fuel was $N_2$ diluted

to reduce soot concentrations in the flame and consequent difficulties with the measurements and with uncertainties in the model due to soot radiation, scrubbing of hydrocarbons by soot, and so on. The fuel and air velocities at the burner surface were a uniform 35 cm/s independent of $R$ (i.e., they had top-hat profiles); physically this was realized by having a honeycomb cover the entire top surface of the burner. The flame was unconfined, and the flow was laminar.

The combination of $N_2$ fuel dilution, a narrow fuel tube, and a high air flow rate caused the flame to be lifted approximately 6 mm above the burner surface. This prevented heat transfer from the flame to the burner and consequent preheating of the reactants. Thus, the thermal boundary condition at the burner surface was well defined (the reactant temperature equaled room temperature at all values of $R$), which is crucial to obtaining good agreement between the model and experiments [8,9].

### *Computer Model*

The flame was modeled by solving the full set of elliptic equations for the conservation of total mass, momentum, energy, and individual species mass. Detailed transport coefficients and a finite-rate $C_1$ to $C_6$ kinetic mechanism with 140 chemical reactions and 39 chemical species were used. The chemical kinetic mechanism, described in Ref. [10], is a modified version of that used by Smooke and coworkers [11], with additional $C_3$ to $C_6$ chemistry derived from Ref. [12,13]. The system was closed with the ideal gas law and appropriate boundary conditions on each edge of the computational domain. We also included an optically thin radiation model and assumed that for this essentially soot-free flame the only radiating species were $H_2O$, CO, and $CO_2$ [14]. The governing equations were written in primitive variables and solved using Newton's method with pseudo-time integration on a non-staggered grid [15].

### *Rayleigh-Raman Imaging*

Two-dimensional images of temperature and major species ($N_2$, $CO_2$, $CH_4$, $H_2$, $O_2$, CO, and $H_2O$) mole fractions were measured using vibrational Stokes-shifted Raman scattering and Rayleigh scattering [1,16,17].

The scattering was excited with the 532-nm harmonic of a 10-Hz Q-switched Nd:YAG laser which was focused into a 300-$\mu$m beam-waist line over the center of the burner. The laser was double-pulsed, with pulse separations of 100 $\mu$s and an average energy of 150 mJ per pulse, to prevent air breakdown over the burner. Measurements were performed from $Z = 0.2$ to 5.4 cm, in steps of 0.05 cm closer to the burner surface and 0.1 cm further downstream. These line measurements were then tiled together to form images. Each measurement was an integration over 1000 double laser pulses to obtain adequate signal-to-noise ratios.

The scattered light was collected with a $f/1.8$ camera lens, rotated 90° by a pair of mirrors placed behind the lens, and focused onto the 700 $\mu$m wide vertical entrance slit of a 0.27 m, $f/4$ imaging spectrograph. The spectrograph dispersed the Rayleigh line and Stokes-shifted Raman lines and focused them onto a gated, image-intensified, cooled charge-coupled device (CCD) camera (1 $\mu$s gate time). The spatial resolution was $\approx 200$ $\mu$m in the radial direction, and the spectral resolution was $\approx 3$ nm. The Raman lines for each species and the Rayleigh line were integrated spectrally over a window large enough to account for the spectral broadening due to temperature increases, but small enough to minimize cross talk with neighboring species.

Fluorescence from $C_2$ and polycyclic hydrocarbons interfere with Raman signals measured on the fuel-rich side of flame fronts [18]. These interferences were reduced to their shot noise levels by taking the difference of the detected light intensities under two orthogonal linear polarizations that were parallel ($I_{zz}$) and perpendicular ($I_{yz}$) to the linearly polarized laser source. A modified liquid crystal shutter was used as a programmable polarizer, which enabled us to measure $I_{zz}$ and $I_{yz}$ independently.

The images were corrected for throughput and spectral efficiency using room temperature air and $CH_4$ calibrations, for laser energy variation, and for cross talk between species. Calibrations of relative Raman cross sections were obtained at room temperature and in a premixed flat flame. The temperature dependence of Raman cross sections was modeled for all species [19,20], and the depolarization of the Raman signals was taken into account. An iterative technique, which usually converged in three iterations, was used to determine species mole fractions and temperature.

### *Thermocouples and On-Line Mass Spectrometry*

The thermocouple measurements employed uncoated 75 $\mu$m wire-diameter type R thermocouples, were corrected for radiation heat-transfer losses, and had an absolute uncertainty of 50 K and a relative uncertainty of 10 K [21]. Species concentrations were determined by extracting gas samples from the flames with a narrow-tipped quartz gas sample probe and analyzing them via on-line mass spectrometry [22]. A custom-built single-photon 118.2 nm photoionization/time-of-flight mass spectrometer (PTMS) was used to measure $C_3$ to $C_{12}$ hydrocarbon mole fractions, and a commercial 70 eV electron-impact/quadrupole mass spectrometer (EQMS; Stanford Research Systems RGA100) was used to

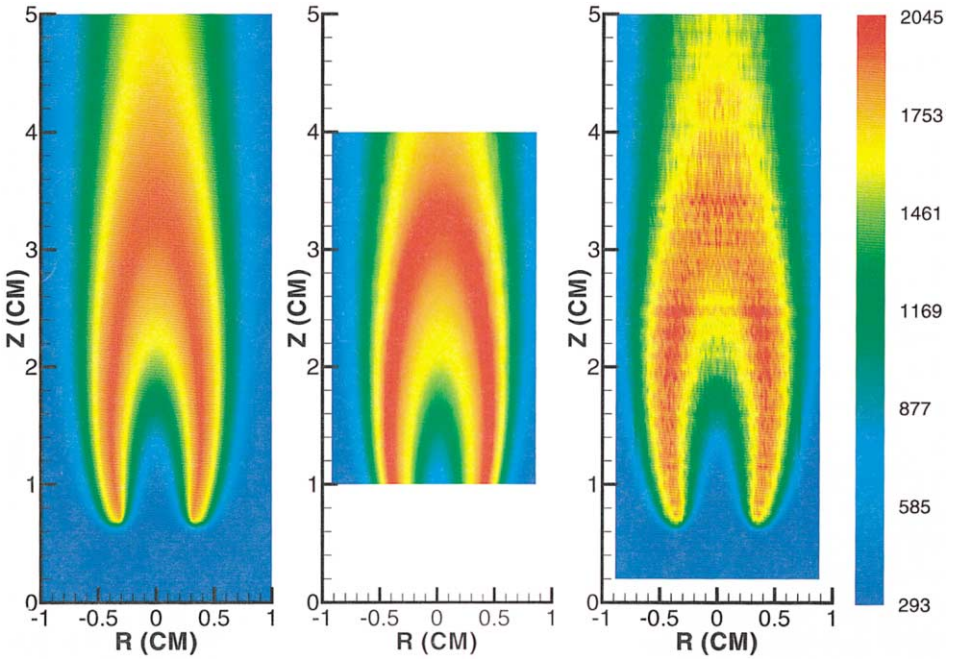


FIG. 1. Comparison of model (left), thermocouple (middle), and Rayleigh-scattering (right) gas temperatures.

measure acetylene and several major species. The relative uncertainties for all species and the absolute uncertainties for acetylene and benzene were 30%, while the absolute uncertainties for other hydrocarbons were up to a factor of 3 [22].

## Results and Discussion

Contour plots of some of the computed and measured results are shown in Fig. 1–10. In these figures, the horizontal and vertical directions correspond to the horizontal and vertical coordinates in the flame, the vertical centerline of each panel corresponds to the centerline of the flame, the bottom edge of each panel corresponds to the burner surface, and the temperatures or mole fractions at each flame location are represented by a color, as indicated by the color scale to the far right in each figure. The same color scale is used for all of the panels in each figure. Most of these figures are arranged with the computational results in the left-hand panel, the thermocouple or mass spectral results in the middle panel, and the Rayleigh-Raman results in the right-hand panel. For $CH_4$, $H_2O$, CO, and $H_2$, only computational and Rayleigh-Raman results are shown (left and right panels, respectively), while for the non-fuel hydrocarbons, only computational and mass spectral results are available (left and right panels, respectively).

Neither of the experimental data sets extends all the way to the burner surface. When the thermocouple and gas sample probe were below $Z = 1$ cm, the flame tended to attach to them, so no reasonable data could be acquired, and this region is blank in all of the figures. However, when they were raised above $Z = 1$ cm, the flame visibly detached and assumed its unperturbed position; the good agreement between the thermocouple/mass spectral and Rayleigh-Raman measurements indicates that the thermocouple and sample probe negligibly perturb the flame above 1 cm. Rayleigh-Raman measurements could not be acquired within 0.2 cm of the burner surface due to reflections of the laser. Flame perturbations are not an issue for these optical measurements; this is one of their major benefits.

### *Gas Temperatures*

The spatial distributions of the temperatures agree very closely among the computations and both sets of experiments (Fig. 1). In all three cases, the high-temperature regions have a wishbone structure; since the fuel flows upward from the burner surface between $R = 0.2$ and $-0.2$ cm, and the air from $R > 0.2$ and $< -0.2$ cm, the lower portion of the wishbone corresponds to the reactive interface between the fuel and air streams, and the upper portion of the wishbone corresponds to the hot products that are being convected downstream and are slowly

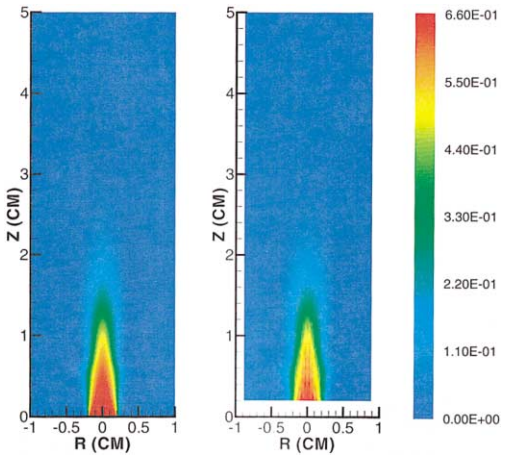


FIG. 2. Comparison of model (left) and Raman-scattering (right) methane mole fractions.

cooling. The flame heights, defined by where the maximum temperature occurs on the centerline, are 3.18, 3.4, and 3.25 cm for the computations, thermocouple measurements, and Rayleigh-Raman measurements, respectively.

The most notable discrepancy among the data sets is that the thermocouple temperatures are substantially higher than the other results in the cool core inside the flame front (i.e., on the centerline at Z = 1 cm). This difference is likely a consequence of heat conduction along the wire, which was stretched through the flame parallel to the burner surface and thus exposed to very large temperature gradients in this part of the flame. Thus, the ability of the Rayleigh-Raman measurements to make accurate measurements in this region again illustrates the advantage of the non-perturbing optical approach. However, the gradients in the core of this lifted flame are much larger than those encountered in non-lifted non-premixed flames, where we have shown that conduction errors can be made negligible [21].

The maximum temperatures are 1946, 2045, and 1982 K for the computations, thermocouple measurements, and Rayleigh-Raman measurements, respectively. The higher maximum temperature for the thermocouple measurements is a discrepancy that was also observed in an earlier comparison with thermocouple measurements from a different group [23] and that we have also observed in ethylene flames [9].

The computational and Rayleigh-Raman temperatures both clearly illustrate that the flame is lifted from the burner surface. In each case the temperatures are very close to room temperature from the burner surface to Z ≈ 0.6 cm, then abruptly rise to near their maximum value in only a few tenths of a centimeter. The specific liftoff heights for the computational and Rayleigh-Raman results clearly agree very closely.

### *Major Species*

As with the temperature results, the agreement among the computations and the two experimental data sets for the major species is very good, both in terms of the spatial structure and the maximum concentrations. All of the results show the expected behavior for a non-premixed flame, with $CH_4$ inside the flame front and $O_2$ outside it (Figs. 2, 3), and with the fuel being converted first to CO and $H_2$ (Figs. 4, 5) and then to $CO_2$ and $H_2O$ (Figs. 6, 7). However, both the computational and Rayleigh-Raman results show that while $H_2O$ formation begins quickly, formation of $CO_2$ is delayed until all of the fuel has been consumed. This occurs because hydrocarbons react more rapidly with OH than does CO, thus inhibiting CO to $CO_2$ oxidation [7].

The Rayleigh-Raman images in Figs. 1–7 have much greater signal-to-noise ratios than those presented earlier [1]. This improvement demonstrates the value of using polarization information to suppress fluorescence interferences and presents a much more stringent test of the computational results. For example, $O_2$ entrainment at the flame base was not detectable in the earlier experimental measurements but is clearly evident in Fig. 3, and its shape and magnitude are well predicted by the model. Similarly, both the computational and Rayleigh-Raman results show a slight outward-facing kink in the methane images at the height where the flame begins to burn (Z = 0.6 cm).

CO and $H_2$ are more difficult to measure with Rayleigh-Raman scattering than other major species due to their low concentrations and overlap with $C_2$ fluorescence bands; thus the CO and $H_2$ images contain more noise than the others (Figs. 4, 5). Nonetheless, the images indicate that the magnitudes and spatial distributions predicted by the model for these species are accurate.

Although the probe measurements do not extend that close to the burner surface, they also show $O_2$ entrainment at the centerline (Fig. 3). Furthermore, the spatial structure of the probe $CO_2$ measurements agrees closely with that of the *in situ* Rayleigh-Raman measurements. Thus we conclude that probe disturbances to the flame are not significant, and the spatial information obtained from the probe measurements of non-fuel hydrocarbons (next section) is trustworthy.

### *Non-Fuel Hydrocarbons*

Figures 8–10 show the results for three non-fuel hydrocarbons, acetylene ($C_2H_2$), benzene ($C_6H_6$),

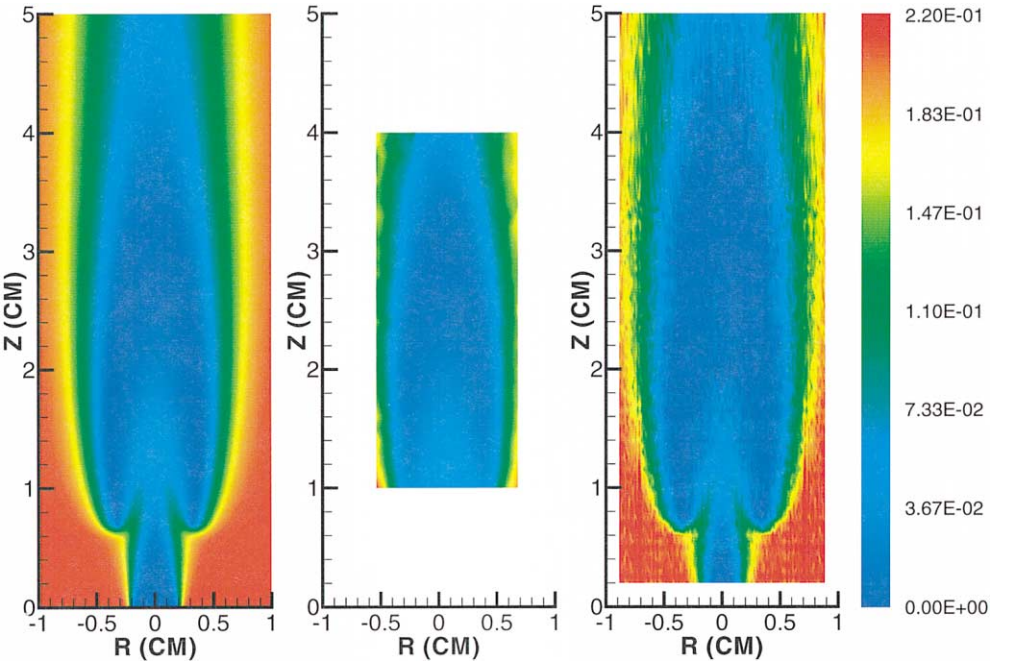


FIG. 3. Comparison of model (left), mass spectrometric (middle), and Raman-scattering (right) oxygen mole fractions.

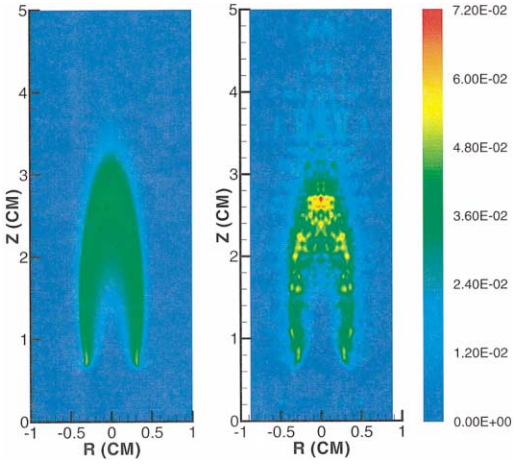


FIG. 4. Comparison of model (left) and Raman-scattering (right) carbon monoxide mole fractions.

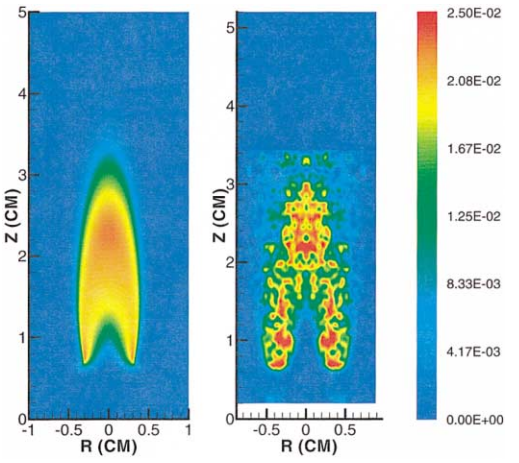


FIG. 5. Comparison of model (left) and Raman-scattering (right) hydrogen mole fractions.

and ketene ($CH_2CO$). Acetylene and benzene are important precursors to soot, while ketene is an important oxidation intermediate. The mass spectral results for ketene contain some interference from propene ($C_3H_6$), but this was shown to be a small contribution in previous work [24]. The absolute concentrations of the ketene data are accurate only to within a factor of 3, since a suitable calibration standard was not available. However, since as far as we know, ketene has never been measured at all in a non-premixed flame, let alone mapped in two dimensions and compared with model results, these results are a significant advance.

The agreement between the computational and mass spectral results for these species is quite good. The maximum computed and measured mole

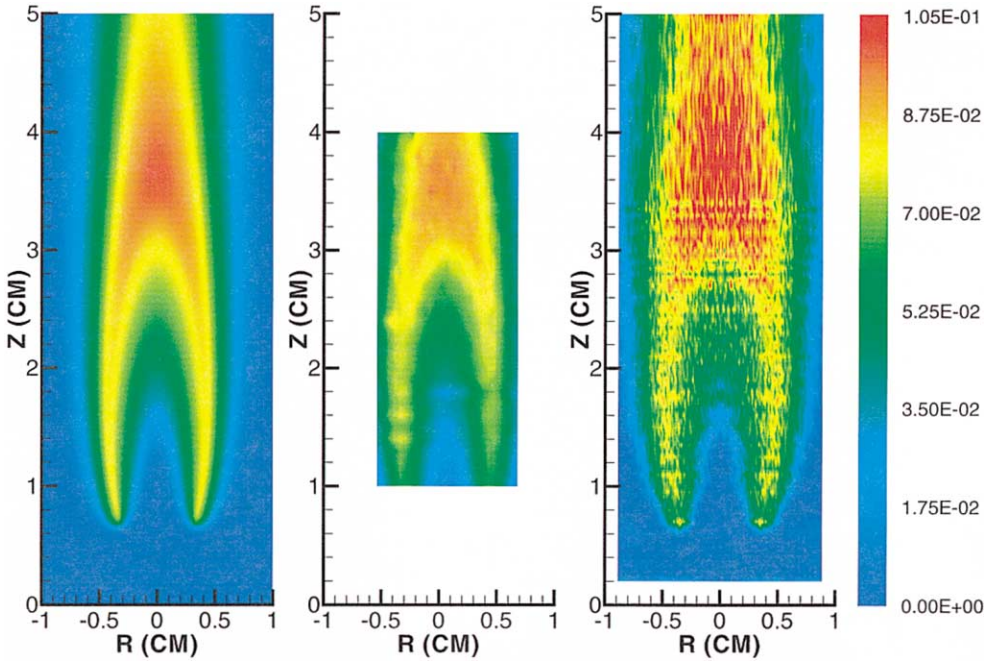


FIG. 6. Comparison of model (left), mass spectrometric (middle), and Raman-scattering (right) carbon dioxide mole fractions.

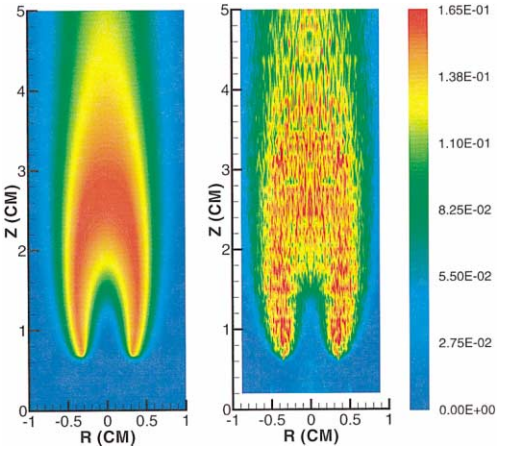


FIG. 7. Comparison of model (left) and Raman-scattering (right) water mole fractions.

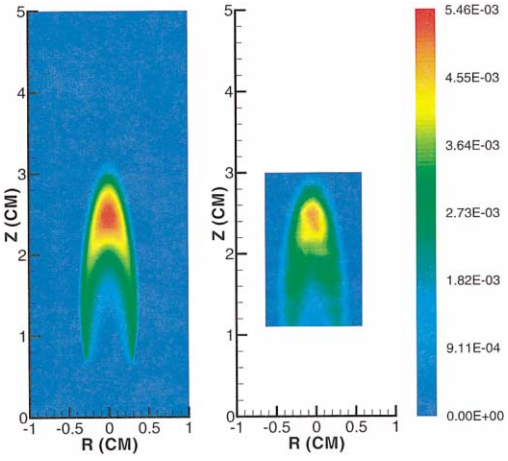


FIG. 8. Comparison of model (left) and mass spectrometric (right) acetylene mole fractions.

fractions for all three agree to within experimental error (72 versus 63 ppm for benzene, 5460 versus 4910 ppm for acetylene, and 36 versus 74 ppm for ketene). The height in the flame where the maximum occurs on the centerline is predicted within experimental error except for ketene, where it is 0.4 cm higher in the computational results. In all of the computational results, the wings of the high concentration contours extend further toward the burner surface than in the experimental results, but this may be a consequence of the finite spatial resolution of the quartz microprobe (0.1 cm). Interestingly, the wings extend the furthest and the least for the same species in both sets (ketene and benzene).

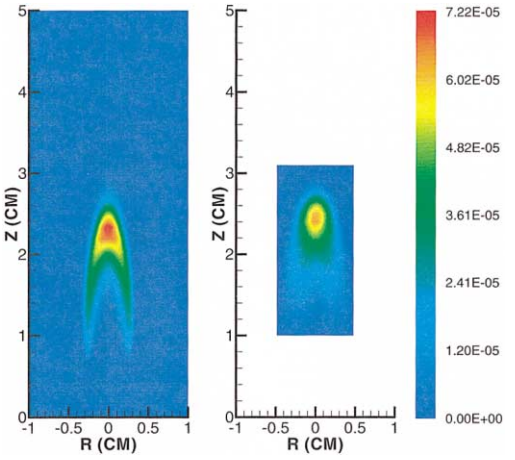


FIG. 9. Comparison of model (left) and mass spectrometric (right) benzene mole fractions.

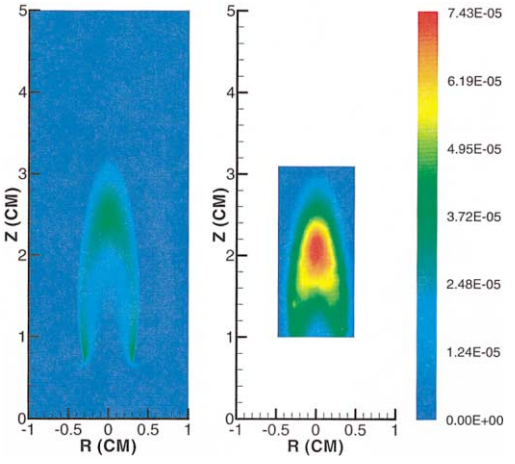


FIG. 10. Comparison of model (left) and mass spectrometric (right) ketene mole fractions.

## Conclusion

This study shows that a coflowing non-sooting non-premixed flame can be well characterized using computational, mass spectrometric, and Rayleigh-Raman techniques. This combined approach allows measurements to be cross-verified and provides a stringent test for model development. The Rayleigh-Raman measurements have been improved significantly by measuring the difference between two orthogonal polarizations, which reduces fluorescence interferences from species on the rich side of the flame front. Computations predicted major and minor species to within experimental error over most of the parameter range, and the agreement on flame structure was equally good with both flame height and liftoff predicted to within several percent.

*Acknowledgments*

We acknowledge financial assistance from the U.S. Air Force, Environmental Protection Agency, Department of Energy, and National Science Foundation.

## REFERENCES

1. Smooke, M. D., Lin, P., Lam, J. K., and Long, M. B., *Proc. Combust. Inst.* 23:575–582 (1990).
2. Seshadri, K., Mauß, F., Peters, N., and Warnatz, J., *Proc. Combust. Inst.* 23:559–566 (1990).
3. Leung, K. M., and Lindstedt, R. P., *Combust. Flame* 102:129–160 (1995).
4. Shu, Z., Krass, B. J., Choi, C. W., Aggarwal, S. K., Katta, V. R., and Puri, I. K., *Proc. Combust. Inst.* 27:625–632 (1998).
5. Zhu, X. L., Nishioka, M., and Takeno, T., *Proc. Combust. Inst.* 27:1369–1376 (1998).
6. Najm, H. N., Knio, O. M., Paul, P. H., and Wyckoff, P. S., *Combust. Sci. Technol.* 140:369–403 (1998).
7. Westbrook, C. K., and Dryer, F. L., *Prog. Energy Combust. Sci.* 10:1–57 (1984).
8. Smooke, M. D., McEnally, C. S., Pfefferle, L. D., Hall, R. J., and Colket, M. B., *Combust. Flame* 117:117–139 (1999).
9. McEnally, C. S., Schaffer, A. M., Long, M. B., Pfefferle, L. D., and Smooke, M. D., *Proc. Combust. Inst.* 27:1497–1505 (1998).
10. Mohammed, R. K., "Computational Study of Steady and Forced, Time-Varying, Axisymmetric, Laminar, Methane-Air Diffusion Flames Using Primitive Variable Formulation with Non-Staggered Grids," Ph.D. thesis, Yale University, New Haven, CT, 1998.
11. Smooke, M. D., Xu, Y., Zurn, R. M., Lin, P., Frank, J. H., and Long, M. B., *Proc. Combust. Inst.* 24:813–821 (1992).
12. Sun, C. J., Sung, C. J., Wang, H., and Law, C. K., *Combust. Flame* 107:321–335 (1996).
13. Wang, H., and Frenklach, M., *Combust. Flame* 110:173–221 (1997).
14. Hall, R. J., *J. Quant. Spectros. Radiat. Transfer* 49:517–523 (1993); 51:635–644 (1994).
15. Mohammed, R. K., Tanoff, M. A., Smooke, M. D., Schaffer, A. M., and Long, M. B., *Proc. Combust. Inst.* 27:693–702 (1998).
16. Reckers, W., Huwel, L., Grunefeld, G., and Andresen, P., *Appl. Opt.* 32:907–918 (1993).
17. Maran, D. F., "Quantitative Two-Dimensional Laser Diagnostics in Idealized and Practical Combustion Systems," Ph.D. thesis, Yale University, New Haven, CT, 1997.

18. Beretta, F., Cincotti, V., D'Alessio, A., and Menna, P., *Combust. Flame* 61:211–218 (1985).
19. Miles, P., *Carbon Dioxide Spectral Synthesis Code,* Sandia National Laboratories, Livermore, CA, 1996.
20. Hassel, E. P., *RAMSES Spectral Synthesis Code,* University of Darmstadt, Darmstadt, Germany 1996.
21. McEnally, C. S., Köylü, Ü. Ö., Pfefferle, L. D., and Rosner, D. E., *Combust. Flame* 109:701–720 (1997).
22. McEnally, C. S., Pfefferle, L. D., Mohammed, R. K., Smooke, M. D., and Colket, M. B., *Anal. Chem.* 71:364–372 (1999).
23. Norton, T. S., Smyth, K. C., Miller, J. H., and Smooke, M. D., *Combust. Sci. Technol.* 90:1–34 (1993).
24. McEnally, C. S., and Pfefferle, L. D., *Combust. Flame* 118:619–632 (1999).